Available online at www.sciencedirect.com
ScienceDirect
Polymer 48 (2007) 4950–4965
polymer
www.elsevier.com/locate/polymer

Honeycomb structured porous films from amphiphilic block copolymers prepared *via* RAFT polymerization

Kok Hou Wong, Thomas P. Davis, Christopher Barner-Kowollik, Martina H. Stenzel*

Centre for Advanced Macromolecular Design (CAMD), School of Chemical Sciences and Engineering, The University of New South Wales, Sydney NSW 2052, Australia

Received 2 March 2007; received in revised form 25 May 2007; accepted 14 June 2007
Available online 27 June 2007

Abstract

The synthesis of polystyrene-*block*-poly(*N*,*N*-dimethylacrylamide) (PS-*b*-PDMA) *via* RAFT polymerization was investigated in detail. Two different RAFT agents – benzyl dithiobenzoate and 3-(benzylsulfanylthiocarbonylsufanyl) propionic acid, were employed to prepare polystyrene macroRAFT agents with molecular weights varying between 3000 g mol^{-1} and 62,000 g mol^{-1} and polydispersities between 1.1 and 1.4. Chain extensions with *N*,*N*-dimethylacrylamide (DMA) were carried out using a constant monomer to RAFT agent concentration ([DMA]/[RAFT] = 500), to compare the rate of polymerization in dependency of the polystyrene chain length. A decreasing rate of polymerization with increasing block length was observed. Depending on the sizes of the first block and type of RAFT agents used, chain extension polymerization with DMA was found to be incomplete, leading to significant low molecular weight tailing in the GPC analyses. Block copolymers prepared using 3-(benzylsulfanylthiocarbonylsufanyl) propionic acid, followed the expected molecular weight evolutions with polydispersity indices of 1.2–1.4. In contrast, block copolymers using benzyl dithiobenzoate clearly showed bimodal molecular weight distributions, especially when the longest PS macroRAFT agent with a molecular weight of 38,000 g mol^{-1} was employed. These amphiphilic block copolymers were used to fabricate honeycomb structured porous films using the breath figure technique. The regularity of the film was considerably influenced by the humidity of the environment, which could be controlled by the rate of the airflow or the humidity in the casting chamber. The interaction between the hydrophilic block copolymer and the humidity was found responsible for the delicate equilibrium during the casting process, which prevented high pores regularity at very low (below 50%) and at elevated (above 80%) humidity. The interactions of the hydrophilic block with the humidity were observed to superimpose an additional nano-scaled order onto the hexagonal micron-sized porous array. Pores, which are created by encapsulation of water droplets, were found to be more hydrophilic than the surface. Confocal microscopy studies were employed to locate hydrophilic blocks within the film using a fluorescence labeled PDMA polymer.

Keywords: Amphiphilic block copolymer; Honeycomb; RAFT

1. Introduction

Highly regular porous films have received increasing interests due to their potential applications as membranes, microreactors and in photonic or opto-electronic devices. Several fabrication methodologies have recently been described in literature for the formation of isoporous films, such as lithographic methods and templating techniques. François and coworkers [1] first described the formation of honeycomb structured porous films by a simple casting method involving breath figures. In this process, water droplets from a humid environment condense on the surface of the polymer solution, giving rise to the appearance of so-called breath figures. Polymers surrounding these water droplets precipitate and form solid envelopes. The water droplets therefore act as templates for these inverse opal structures [2–4]. The hexagonal arrangement of pores and the pore sizes, ranging between 20 nm [5] and 20 μm [6], are influenced by the polymers used and the casting conditions under which the formation

* Corresponding author. Tel.: +61 2 9385 4344; fax: +61 2 9385 6250.
E-mail address: camd@unsw.edu.au (M.H. Stenzel).

0032-3861/$ - see front matter
doi:10.1016/j.polymer.2007.06.048

of films were completed. A variety of polymers have been employed in the preparation of honeycomb structured porous films including polystyrene star or comb polymers [7], rod-coil polymers [8], conjugated polymers with semi-conducting properties [9–11], polyimides [12], light-emitting polymers [13], liquid-crystalline polymers [14], organometallic polymers [15] and degradable polymers such as poly(ε-caprolactone) [16]. When amphiphilic block copolymers [17,18] are used in this process, the formation of a nano-scaled suborder is observed. The precipitation of amphiphilic block polymers around water droplets yielded pores with high hydrophilicity while the film surface remains mostly hydrophobic. These suborder arrangements have been confirmed using XPS [19], contact angle measurements [20] and bacterial studies [3]. Amphiphilic block copolymers could potentially be utilized to generate micron-sized reactors with hydrophilic and functional groups located mainly inside the pores.

RAFT polymerization [21–23] is a versatile technique to synthesize amphiphilic block copolymers without the necessity of protecting the functional groups during polymer synthesis. The formation of polymeric macroRAFT agents with thiocarbonylthio end groups, as a result of the homopolymerization in the presence of a RAFT agent, can be considered as the key component to the successful formation of block copolymers. The so-called macroRAFT agent can then be reinitiated with a new monomer leading to the formation of diblock copolymers (Scheme 1). Detailed investigations into the mechanism revealed that besides diblock copolymers the formation of homopolymers (Scheme 1, IV/(b)) or tri-block copolymers (Scheme 1, (V)) by terminations can be expected during RAFT polymerizations.

A crucial step in the successful formation of block copolymers is the stability assessment of the macro-radical of both polymer blocks. The intermediate radical of the pre-equilibrium phase (Scheme 1, (II)) is the focus when designing a preparative strategy. The fragmentation of this intermediate compound can proceed towards either directions, forming either a macro-radical based on the monomer of the original macroRAFT agent P(M_1) or a macro-radical based on the new monomer P(M_2) [24]. A complete formation of P(M_1) macro-radical is essential for the successful generation of block copolymers while a fragmentation forming P(M_2) macro-radical can only yield homopolymers [25]. The formation of the initial polymer block, with macro-radicals of higher stability, promotes the leaving ability of the macroRAFT agent and consequently leads to the formation of block copolymers. It is therefore recommended to prepare methacrylate-based polymers before carrying out the chain extension polymerization process using acrylates or styrene [26]. A range of well defined amphiphilic block copolymers have been reported using this technique [24–30].

In this paper, systematic investigations into the synthesis of amphiphilic block copolymer, polystyrene-*block*-poly(*N*,*N*-dimethylacrylamide) (PS-*b*-PDMA), were carried out focusing on the influence of the sizes of the first polymer block used in the chain extension polymerization process with DMA. Furthermore, the set of block copolymers prepared was utilized to generate honeycomb structured porous films using the airflow technique [31]. Influences of block size and ratios on the casting process, arrangement and sizes of pore generated were also investigated.

2. Experimental section

2.1. Materials

The synthesis of benzyl dithiobenzoate **I** [32] and 3-(benzylsulfanylthiocarbonylsulfanyl) propionic acid **II** [7] was

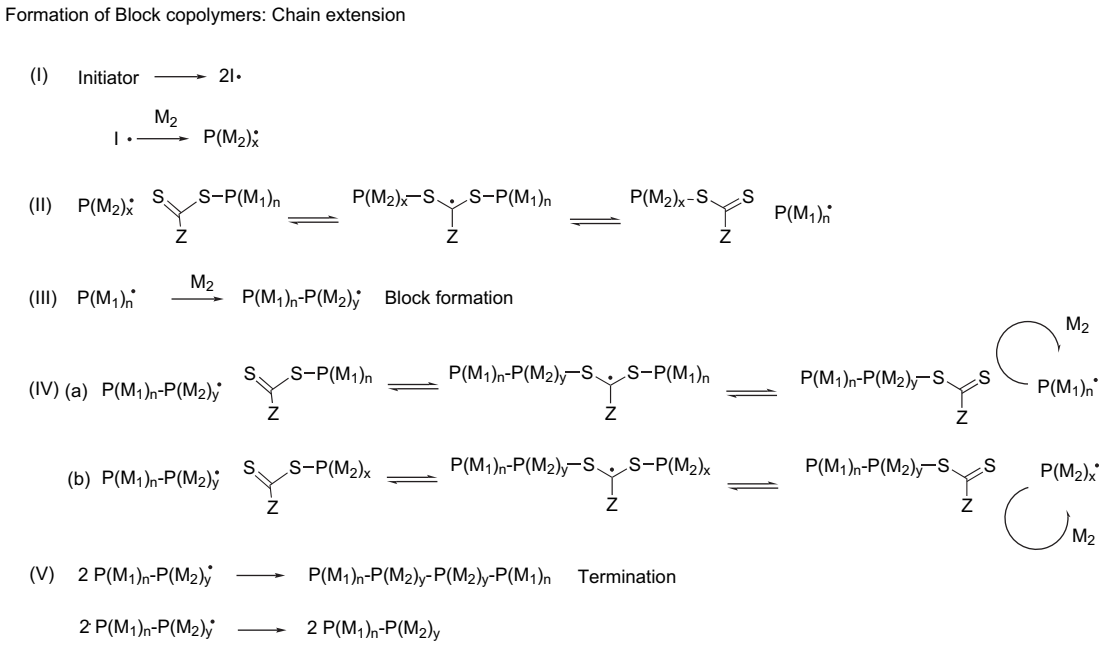

Scheme 1.

described elsewhere. Styrene (S, 99%) and *N*,*N*-dimethylacrylamide (DMA, 99%) purchased from Sigma were destabilized by several passes through columns of basic alumina. *N*,*N*-Dimethylacetamide (DMAc, HPLC) was purchased from Sigma and used without further purifications. 2,2-Azobisisobutylonitrile (AIBN) from DuPont was recrystallized twice with ethanol before use. Carbon disulfide (CS_2, 99.9%) from Ajax Chemicals and dichloromethane (CH_2Cl_2, 99.5%) from Ajax Finechem were used as solvents for casting polymer solutions without further purification.

2.2. Synthesis

2.2.1. Polystyrene macroRAFT agents

Polystyrene macroRAFT agents (PS-**I**), with dithioester end group, of molecular weights 3000 g mol^{-1}, 9000 g mol^{-1} and 38,000 g mol^{-1} were synthesized using the experimental procedures described elsewhere [32]. Polystyrene macroRAFT agents (PS-**II**), with trithiocarbonate end group, of molecular weights of 8000 g mol^{-1}, 33,000 g mol^{-1} and 62,000 g mol^{-1}, respectively, were synthesized by mixing 38 g, 190 g and 380 g of destabilized styrene with 1.0 g of RAFT agent (**II**) – 3-(benzylsulfanylthiocarbonylsulfanyl) propionic acid – respectively, and degassed with nitrogen for 1 h before polymerizing at 100 °C for 48 h while stirring. After polymerization, the mixtures were quenched and excess monomers were removed under reduced pressure. The samples were dried under high vacuum at 50 °C before use.

2.2.2. RAFT polymerization of DMA

PDMA was prepared by mixing 9.913 g, 1×10^{-1} mol of *N*,*N*-dimethylacrylamide – DMA, RAFT agent – benzyl dithiobenzoate **I** (0.0488 g, 2×10^{-4} mol) or 3-(benzylsulfanylthiocarbonylsufanyl) propionic acid **II** (0.0544 g, 2×10^{-4} mol) and AIBN (0.0033 g, 2×10^{-5} mol) with *N*,*N*-dimethylacetamide – DMAc (to obtain a final volume of 50 mL) in a Schlenk flask. The flask was sealed with septa and degassed with three or more freeze–pump–thaw cycles. After degassing the mixture was transferred *via* a canula into several thoroughly degassed bottles sealed with septa and copper wire ties. Polymerizations were carried out at 60 °C. At regular intervals, depending on conversion required, a bottle from each sample set was removed from the water bath, quenched and the solvent was allowed to evaporate. The conversion was determined gravimetrically.

2.2.3. Amphiphilic diblock copolymer (PS-b-PDMA)

As depicted in Scheme 2, polystyrene-*block*-poly(*N*,*N*-dimethylacrylamide), PS-*b*-PDMA, with dithioester end groups: 1.20 g (3000 g mol^{-1}), 3.60 g (9000 g mol^{-1}) or 15.2 g (38,000 g mol^{-1}) polystyrene macroRAFT agent (PS-**I**) (2×10^{-4} mol) was mixed with 9.91 g (1×10^{-1} mol) *N*,*N*-dimethylacrylamide – DMA, 0.00328 g AIBN (2×10^{-5} mol) and *N*,*N*-dimethylacetamide (DMAc) to obtain a final volume of 50 mL, sealed with septa/copper wires and degassed with three or more freeze–pump–thaw cycles. After degassing the mixture was transferred *via* a canula into several thoroughly degassed bottles sealed with septa and copper wire. The polymerization was carried out at 60 °C. At regular intervals a bottle was removed. After evaporation of excess solvent and monomers the conversion was determined gravimetrically. Polystyrene-*block*-poly(*N*,*N*-dimethylacrylamide), PS-*b*-PDMA, with trithiocarbonate end groups, were prepared employing a similar procedure as above using polystyrene macroRAFT agents (PS-**II**) with molecular weights of 8000 g mol^{-1}, 33,000 g mol^{-1} or 62,000 g mol^{-1}.

2.2.4. Casting/porous film formation

A ratio of 70:30 v/v% of CS_2 to CH_2Cl_2 was used for film casting. This solvent mixture was used to aid solubility of polymers, especially those with lengthy PDMA blocks which are partially insoluble in CS_2. Honeycomb structured porous film formation was conducted in a customized Perspex glove box with controlled airflow, temperature and humidity. Castings of porous films were done according to the airflow technique described elsewhere [31]. Polymer solutions of 12–20 μL, dispensed from a precision micro-pipette were introduced onto 5 mm diameter round glass cover-slips within the Perspex box and allowed to evaporate to dry, to yield porous films.

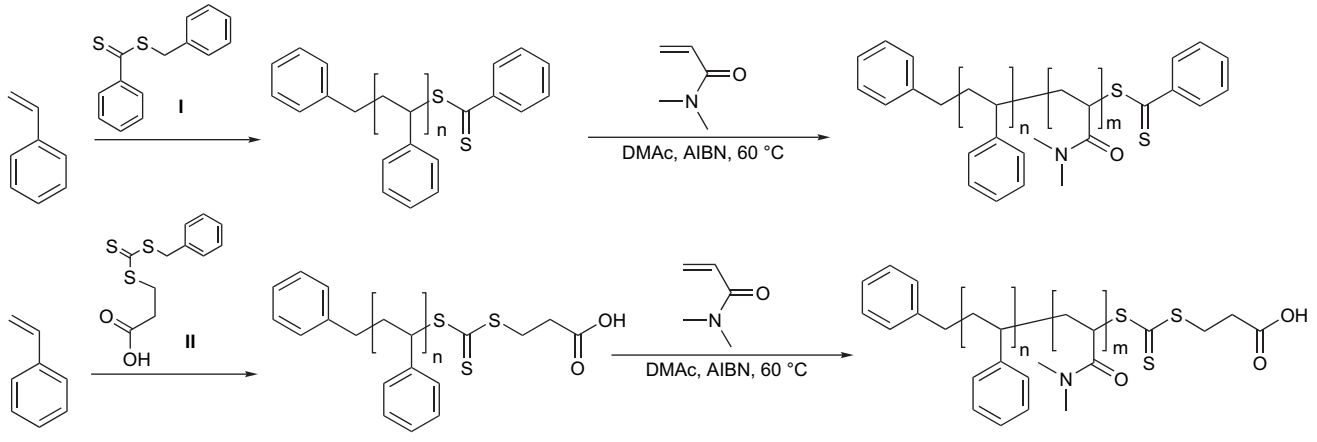

Scheme 2.

3. Characterization

3.1. Gel permeation chromatography (GPC)

Molecular weight analysis of copolymers were performed using size exclusion chromatography (SEC) in a Shimadzu modular LC system comprising of a DGU-12A solvent degasser, an LC-10AT pump, an SIL-10AD auto injector, a CTO-10A column oven (50 °C set temperature), an RID-10A refractive index detector, with *N*,*N*-dimethylacetamide (DMAc) (HPLC, 0.05% w/v LiBr, 0.05% BHT) at a flow rate of 1 mL min^{-1}, as eluent. The system was equipped with a Polymer Laboratories 5.0 μm bead-size guard column (50 × 7.8 mm) followed by four 300 × 7.8 mm linear PL columns (10^5, 10^4, 10^3 and 500 Å). Calibration on the system was performed with narrow polydispersity polystyrene standards ranging from 500 g mol^{-1} to 10^6 g mol^{-1}.

3.2. FT-NIR (Fourier transformed-near infrared) spectroscopy

FT-NIR measurements were performed on a Bruker IFS66\S Fourier transform spectrometer system equipped with a tungsten halogen lamp, CaF_2 beam splitter and a liquid nitrogen cooled InSb detector. Stock solutions in a Schlenk flask, degassed by three or more freeze–pump–thaw cycles were transferred into a rubber septa sealed 10 mm IR cell, deoxygenated by several vacuum–nitrogen cycles, *via* a canula under nitrogen. Monomer conversions were determined *via* online FT-NIR spectroscopy by observing the reduction in vinylic stretching overtone intensity of the monomer at approximately 6140 cm^{-1}. Each spectrum between the spectral regions of 8000–4000 cm^{-1} was calculated from the co-added interferograms of 12 scans with a resolution of 4 cm^{-1}. The conversion was determined, by selecting a linear baseline between 6180 and 6110 cm^{-1} and subsequently, *via* Beer–Lambert's law, the integrated absorbance between these two points was used to calculate the monomer to polymer conversion.

3.3. DLS (dynamic light scattering)

The determination of polymer particle size in dichloromethane solution (10 g L^{-1}) was performed on a Brookhaven Instruments ZetaPals Particle analyser system at room temperature (25 °C), using an angle of 90° and wavelength of 678 nm. ZetaPals particle sizing software (version 3.57) was used to obtain the distributions of hydrodynamic diameter $f(D_h)$ for each measurement.

3.4. SEM (scanning electron microscopy)

Scanning electron microscopy (SEM) analysis of the prepared porous films was performed using a Hitachi S-900 FESEM. The porous film samples were affixed to copper stubs with carbon adhesive tape and sputter-coated with 10 nm of chromium (EMITECH K575× high resolution) prior to analysis.

3.5. Quantitative virtual light scattering (QVLS) analysis

Analysis of the pore profile and size was conducted on SEM images, with the aid of Scion image software (Scion Corporation) release Beta 4.0.2. The coordinates ($X-Y$ positional data) of the pores' geometric centre obtained using Scion image were later used to yield two parameters; SPAN and THETA coefficients, using quantitative virtual light scattering (QVLS) analysis [33]. QVLS employs Fourier transformation to determine the SPAN and THETA coefficients. The SPAN value is the standard deviation of the distance between the centers of two neighboring pores; a small value for this parameter is indicative of a constant positioning of pores. The THETA value is the standard deviation of the angle formed by three neighboring pores; a small value for this parameter indicates an angle of 60° arrangement of the pores, a requirement for a hexagonal assembly [7,33,34].

4. Results and discussion

4.1. Synthesis of polymers

In the synthesis of polystyrene-*block*-poly(*N*,*N*-dimethylacrylamide) (PS-*b*-PDMA) block copolymers, it is essential to generate the polystyrene macroRAFT agent polymer block before chain extension with DMA. Experiments, using PDMA macroRAFT agent first, resulted in incomplete chain extension with styrene, evidenced by a bimodal GPC molecular weight distribution spectrum.

Two RAFT agents, benzyl dithiobenzoate **I** and 3-(benzylsulfanylthiocarbonyl sulfanyl) propionic acid **II** agents were used in this work. Both classes of RAFT agents were tested to convey a living polymerization process with styrene and DMA. Polystyrene macroRAFT agents with varying molecular weights were generated using both RAFT agents. Benzyl dithiobenzoate **I** was employed to generate polystyrene macroRAFT agents (PS-**I**) with molecular weights of 3000 g mol^{-1}, 9000 g mol^{-1} and 38,000 g mol^{-1} while 3-(benzylsulfanylthiocarbonylsulfanyl) propionic acid **II** was utilized to generate polystyrene macroRAFT agents (PS-**II**) with molecular weights of 8000 g mol^{-1}, 33,000 g mol^{-1} and 62,000 g mol^{-1}. All six macroRAFT agents as well as RAFT agents **I** and **II** were employed in the chain extension polymerization and homopolymerizations of DMA, using similar RAFT end group concentrations ([M]/[RAFT] = 500).

Fig. 1A and B reveals that the rates of homopolymerisation of DMA using **I** and **II** deviate considerably from each other. These results were not surprising and can be attributed to an increased stability of the intermediate radical of dithioester mediated polymerization, resulting in strongly retarded polymerizations in the presence of **I** [35].

A significant influence was observed by the chain length of the PS macroRAFT agent used while all other concentrations were kept constant. The chain extension polymerization process was significantly retarded with increasing PS block length. The employment of increasing molecular weight macroRAFT agents resulted in higher viscosity which was known

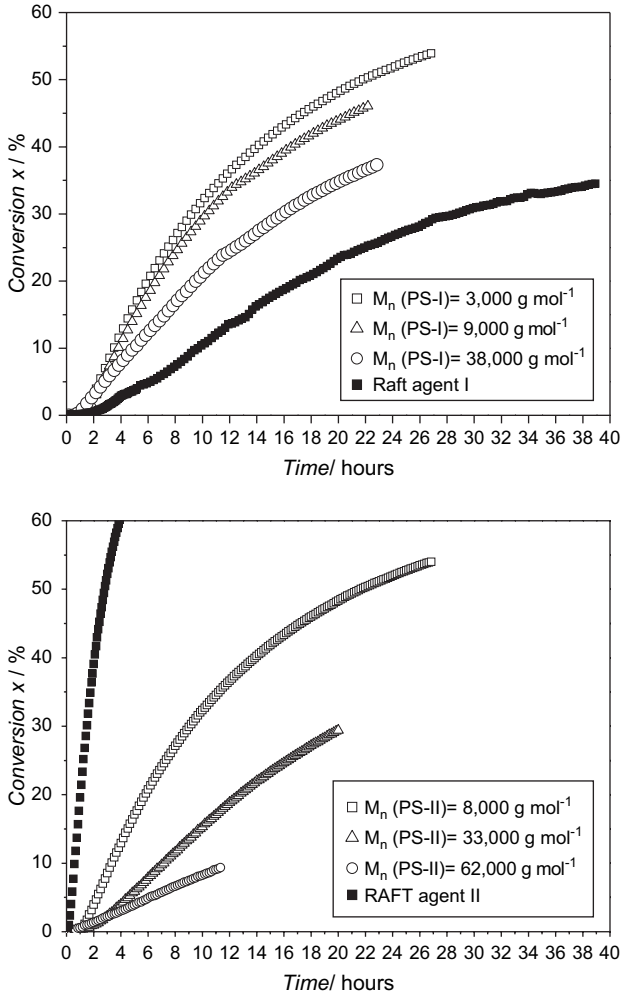

Fig. 1. Time *vs* conversion plots as obtained *via* FT-NIR measurements of the polymerization of *N*,*N*-dimethylacrylamide (DMA) in *N*,*N*-dimethylacetamide (DMAC) at 60 °C in the presence of macroRAFT agents, PS-**I** (above) and PS-**II** (below). Concentrations: [macroRAFT] = 4×10^{-3} mol L^{-1}, [DMA] = 2 mol L^{-1}, [AIBN] = 4×10^{-4} mol L^{-1}.

to affect several parameters during polymerization. Alteration of the viscosity can have manifold influences on the polymerization kinetics such as the decrease of the termination rate coefficient or the decrease of initiator efficiency. A decreased rate of termination, however, results in a faster rate of polymerization and therefore cannot explain the delay in this case. In contrast, increasing the viscosity usually causes lower initiator efficiencies, thus reducing the concentration of radicals in the system. The reduced initiator efficiency and the resulting reduced rate of polymerization can indeed be suspected when using trithiocarbonate based macroRAFT agents (PS-**II**). Fig. 1B shows an amplified retardation with increasing chain length of the polystyrene blocks used. The effect of higher viscosity on the radical concentrations should then be observed during the course of polymerization since the viscosity increases with monomer consumption. Undeniable, the first-order kinetics plot did not follow a linear relationship and exhibit a reduction of radical concentrations, which can either be explained by the decomposition kinetics of AIBN or an altered initiator efficiency.

The peculiar behavior of the DMA polymerization using dithioester based RAFT agent **I** revealed, however, that the influences on the rate of chain extension polymerization of DMA with dithioester based macroRAFT agents (PS-**I**) were considerably more complicated (Fig. 1A). While the polymerization of DMA in the presence of **I** was highly retarded, the rate of polymerization using a polystyrene macroRAFT agent was accelerated. Similar to chain extension polymerizations with trithiocarbonate based macroRAFT agents (PS-**II**), the rate of polymerization was impeded with the length of the polystyrene block employed. Comparing polymerizations using macroRAFT agents (PS-**I**) of varying sizes, a significant increase in the polymerization rate was observed when polymeric RAFT agents were employed. Since the influence of the RAFT agents should be similar, this can only be assigned to either an increased radical concentration or the decreased rates of termination at higher chain lengths. Moreover, the reaction between macro-radical and thiocarbonylthio group may be chain length dependent, which can be a reflection of the altered accessibility of the RAFT end group within the polymer coils. Interestingly, when comparing chain extension polymerizations, using different classes of macroRAFT agents but with comparable polymer block sizes, similar rates of polymerization within acceptable errors were observed (Fig. 2). This may be coincidental, but can also be attributed to similar viscosity effects. Further investigations are necessary to obtain additional information on the chain length dependency of the chain extension RAFT polymerization process.

The homopolymerizations of both monomers (styrene and DMA) using **I** and **II** were confirmed living since the molecular weight evolved linearly with conversion while the molecular weight distribution remained narrow (typically between 1.2 and 1.4 for polystyrene and 1.1 and 1.3 for DMA homopolymerization in the presence of **I** and **II**). The syntheses of block

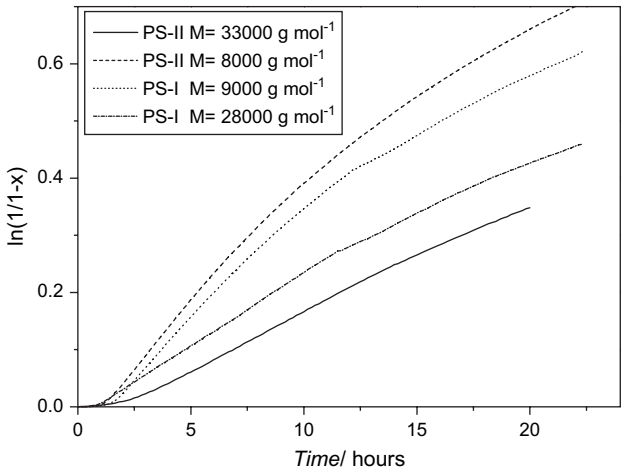

Fig. 2. Pseudo first-order kinetic plot as obtained *via* FT-NIR measurements of the polymerization of *N*,*N*-dimethylacrylamide in *N*,*N*-dimethylacetamide at 60 °C in the presence of varying PS macroRAFT agents (PS-**I** and PS-**II**). Concentrations: [macroRAFT] = 4×10^{-3} mol L^{-1}, [DMA] = 2 mol L^{-1}, [AIBN] = 4×10^{-4} mol L^{-1}.

copolymers, however, were more complicated. As mentioned above, we expect a chain length dependency on the chain transfers during chain extension polymerization. Additionally, it should be considered that we attempt to combine a hydrophilic monomer to a relatively hydrophobic polymer block.

On first inspection, the chain extension of polystyrene block copolymers with DMA, using **II** (Figs. 3 and 4) seems to be complete, showing a monodisperse GPC distribution. The peaks shifted with conversion to higher molecular weight, which were especially pronounced when employing low molecular weight macroRAFT agents. The molecular weights obtained from GPC analysis (using linear polystyrene standards) exhibited a linear increase in molecular weight with conversion. In addition, the molecular weight distributions remained below 1.4. Deviation from the expected molecular weight (solid line in Fig. 4), especially when using longer macroRAFT agents, may be assigned to the polystyrene standard calibrations on the GPC system. Molecular weight differences between the theoretical molecular weight and the measured value can be explained by altered hydrodynamic volumes, which can significantly be affected in complex architectures. However, the observed deviation in this case cannot only be assigned to the GPC calibration. Some strong indications suggest the occurrence of side reactions affecting the molecular weight distribution. Detailed inspections of the GPC curves revealed that a significant low molecular weight tailing appeared which became even more noticeable at higher conversions, especially when using higher molecular weight macroRAFT agents (Fig. 3). To further investigate into this observation, the intensity of the GPC curves were recalculated to take into considerations, that with increasing DMA conversions the intensity of the original polystyrene macroRAFT block was skewed. The intensity of each GPC curve was multiplied with the theoretical number of repeating units of the block copolymer $N_{DMA} + N_{PS}$ and divided by the size of the original

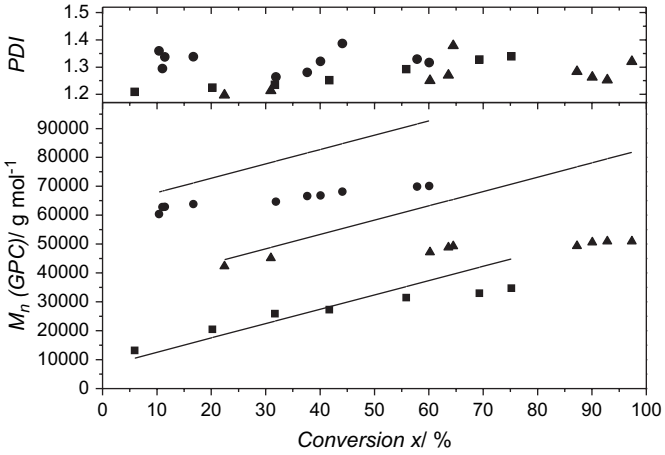

Fig. 4. Molecular weight M_n as obtained *via* GPC (DMAc) and polydispersity index (PDI) of the polymerization of *N*,*N*-dimethylacrylamide (DMA) in *N*,*N*-dimethylacetamide (DMAc) at 60 °C in the presence of varying PS macroRAFT agents (PS-**II**). Concentrations: [macroRAFT] = 4×10^{-3} mol L^{-1}, [DMA] = 2 mol L^{-1}, [AIBN] = 4×10^{-4} mol L^{-1}. The molecular weight of the PS macroRAFT agent is 8000 g mol^{-1} (square), 33,000 g mol^{-1} (triangle) and 62,000 g mol^{-1} (circle).

macroRAFT agent N_{PS}. (It should be noted that this technique can only provide an estimate given that both polymer blocks deviate in their refractive indices.) Fig. 5 depicts, the macroRAFT agent was only consumed slowly during polymerization resulting in diblock copolymers with varying DMA block sizes. Consequently, some block copolymers were generated earlier than others, and eventually yield polymers with bigger DMA blocks. Therefore the tailing becomes increasingly evident and magnified when employing macroRAFT agents of higher molecular weight. It should also be noted here that low molecular weight tailing or a second distinct peak of remaining macroRAFT agent may also be the result of dead polymer generated during the synthesis of the macroRAFT

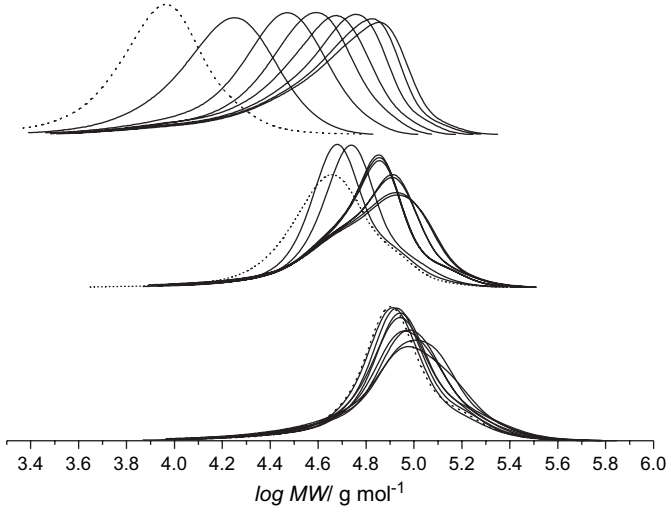

Fig. 3. GPC curves (DMAc) of PS-*b*-PDMA block copolymers using PS macroRAFT agent (PS-**II**) (dotted lines) with molecular weights of 8000 g mol^{-1} (top), 33,000 g mol^{-1} (middle) and 62,000 g mol^{-1} (bottom). Experimental details are listed in Fig. 4.

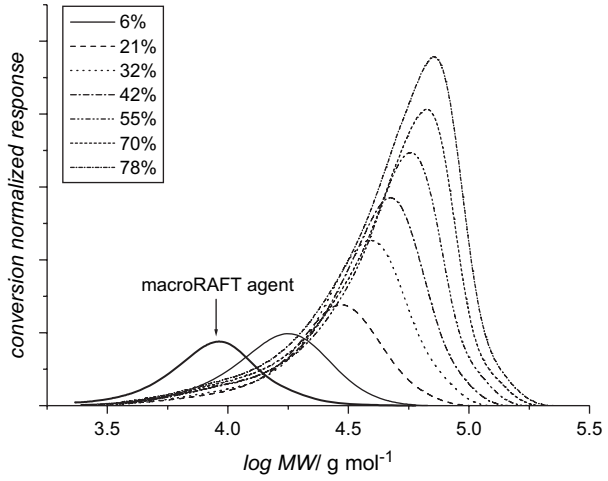

Fig. 5. GPC curves of PS-*b*-PDMA block copolymers based on PS-II ($M_n = 8000$ g mol^{-1}) (above) and PS-I ($M_n = 38{,}000$ g mol^{-1}) (below) obtained by multiplying the normalized response with the conversion and the maximum ratio r at 100% conversion, which is then added onto the original value (N is the number of repeating units); $r = \frac{N_{PDMA}+N_{PS}}{N_{PS}} = \frac{500+77}{77} = 7.5$.

agent. It is well known that certain conditions such as heat [36], light [37], certain pH values [38] and solvents containing oxidizing species like dioxane or tetrahydrofuran [39] can influence or even destroy thiocarbonylthio end groups. In addition dead polymer can be formed during the macroRAFT agent synthesis by an unfavourable high concentration of radicals, which will result in a substantial amount of termination reactions. Dead polymer, however, will not result in the slow consumption of the macroRAFT agent, but will be indicated as a second peak (or low molecular weight tailing) unchanged in intensity (when scaling the GPC curves with the monomer conversion) throughout the polymerization.

This effect was also observed and even more significant when using dithioester based macroRAFT agents (PS-**I**) during chain extension with DMA. The polymerization in the presence of (PS-**I**) (Fig. 6) clearly resulted in a bimodal molecular weight distribution which was again more pronounced with increasing molecular weight of the macroRAFT agent used. The bimodality was evidently a function of the macroRAFT agent molecular weight. The chain extension process using a macroRAFT agent of a molecular weight of 3000 g mol^{-1} showed an initial good extension and almost full chain extension with the second monomer, with the peaks shifting fully to higher molecular weights. The chain extension process using a larger polystyrene macroRAFT block size was clearly incomplete and deviated from the expected molecular weight (solid line in Fig. 7). The broadening becomes now very prominent with a significant increase of the polydispersity (PDI of 2.4). The polydispersity index increased not only with conversion but also with block size (Fig. 7).

In comparison, the chain extension polymerization using PS-**II** did result in the formation of block copolymers despite some noticeable low molecular weight tailing, indicative of a delayed chain transfer process during polymerizations. MacroRAFT agent PS-**I**, in contrast, showed significant broadening

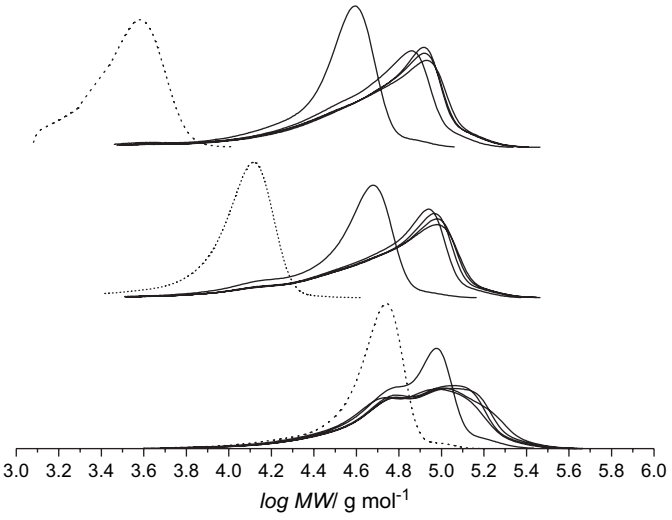

Fig. 6. GPC curves (DMAc) of PS-*b*-PDMA block copolymers using PS macroRAFT agent (PS-**I**) with molecular weights, 3000 g mol^{-1} (top), 9000 g mol^{-1} (middle) and 38,000 g mol^{-1} (bottom). Experimental details are listed in Fig. 7.

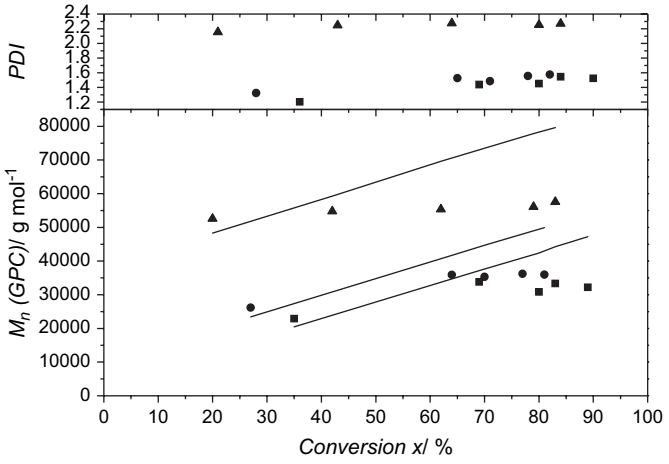

Fig. 7. Molecular weight M_n as obtained *via* GPC (DMAc) and polydispersity index (PDI) of the polymerization of *N*,*N*-dimethylacrylamide in *N*,*N*-dimethylacetamide at 60 °C in the presence of varying PS macroRAFT agents (PS-**I**). Concentrations: [macroRAFT] = 4×10^{-3} mol L^{-1}, [DMA] = 2 mol L^{-1}, [AIBN] = 4×10^{-4} mol L^{-1}. The molecular weight of the PS macroRAFT agent is 3000 g mol^{-1} (square), 9000 g mol^{-1} (circle) and 38,000 g mol^{-1} (triangle).

of the molecular weight distribution especially when the macroRAFT agent reached a certain size. In both cases, we clearly observed a chain length dependency of this effect. It seemed the accessibility of the thiocarbonylthio end group was determined by the size of macroRAFT agents. Additionally, it should be considered that the hydrophobic PS macroRAFT agent is chain extended with a hydrophilic block, which causes repulsive effects [40]. The observed low molecular weight tailing may additionally be explained by the preferred chain extension of a polymer chain that has already undergone chain extension. Hence, the increased hydrophilicity around the thiocarbonylthio group, caused by the addition of a few DMA units, facilitates further chain extension. This polarity effect may also explain the difference between the polymerization using **I** or **II**. RAFT agent **I** is hydrophobic in contrast to the carboxy group carrying RAFT agent **II**. Further investigations are necessary to quantify the potential effects of chain length and polarity on the formation of block copolymers. On the contrary, theoretical modeling studies predicting the decrease of the polydispersity with conversions in block copolymer synthesis [41] are clearly underestimating the effect of polarity and polymer chain conformations.

Nevertheless, the formation of block copolymers using PS-**II** can be considered suitable for the preparation of PS-*b*-PDMA block copolymers since the mono-modal molecular weight distribution never exceed a polydispersity index of 1.4. Likewise, this exercise illustrated that it is essential to investigate the shape of GPC curves when preparing block copolymers *via* RAFT polymerization.

4.2. Honeycomb structured porous films

In this study, honeycomb structured porous films were effectively fabricated by a simple casting process, employing

a polymer solution in a humid environment. The prerequisites for the class of polymer that support the formation of highly regular porous films are nonetheless ambiguous [17]. However, in an empirical fashion it has been shown that an assortment of polymers can be employed successfully. Amphiphilic block copolymers are unique since these structures are expected to interfere with the casting process to produce porous films with interesting morphologies (Scheme 3). The utilization of amphiphilic block copolymers in the preparation of honeycomb structured porous films can lead to a nano-scale suborder with hydrophilic pores. The block size ratios as well as the overall molecular weight of amphiphilic block copolymers employed are expected to have significant influences on the pore size and especially on the regularity of the hexagonal array formed. The aim of this study is to systematically investigate the correlations between the block sizes and block ratios of the polymer used to the outcome of films formed.

The process of casting is highly sensitive towards slight alteration of casting humidity, airflow and temperature. Therefore, a customized Casting Perspex glove box [31], integrated with an adaptable moist air supply system providing control of several physical casting conditions e.g. humidity, temperature, airflow rate and airflow directions was designed and built. With this customized glove box, we were able to complete our castings to generate honeycomb structured porous films under different conditions while achieving reproducible results. For the quality of films produced, the primary focus would be on the topography of porous films, such as pore arrangement pattern (hexagonal fashion), pore size and pore homogeneity. Numerous conditions are assumed to influence the formations of honeycomb structured porous films and were identified as the following:

1. Materials: type of polymer, architecture of polymer, polymer molecular weight.
2. Casting conditions: humidity, temperature, moist airflow rate, moist airflow directions, type of substrate, substrate surfaces, substrate temperature, type of solvent, concentrations of polymer in solvent, solvent temperature, volume of casting.

Investigations into all these conditions are beyond the scope of this study and were discussed in detail elsewhere [2,4,26]. In this work, we focus primarily on parameters, which are unique to amphiphilic block copolymers such as their interaction with water as well as organic solvent. Therefore, the size of the hydrophilic block or the ratio of both blocks, respectively, should significantly influence the pore size and regularity.

4.3. Pre study: interaction of amphiphilic block copolymer with water

As mentioned, the uniqueness of amphiphilic block copolymers lies in their possible interference of the hydrophilic block with condensing water droplets. The formation of inverse micelles in typical casting solvents such as methylene chloride and carbon disulfide can be expected with the hydrophilic PDMA block forming the core. Upon contact with water, two possible reactions can occur: firstly, the block copolymers arrange themselves around the water droplets on the surface. As a result, the surface tension can be altered and the droplets show an increased tendency to coalesce. With increasing size of the hydrophilic block the interfacial tension decreases. Consequently, the coalescence should increase, thus, forming a more irregular array of pores on the resulting film. However, it should be considered that a very high interfacial tension was reported to result in films of lower order, which could be improved by the addition of surface active compounds [17]. Secondly, the micelles can take up substantial amounts of water during the casting process resulting in significantly swollen particles.

To quantify the penetration of water into the micelle, solutions of a range of block copolymers in a typical casting solvent – methylene chloride – were prepared. Both polymer and solvent were dried thoroughly to allow the investigation of the block copolymer in the dry state. The hydrodynamic diameter D_h of the inverse micelle in the solvent at 10 mg mL^{-1} was found to be strongly dependent on both block sizes in particular, the core forming PDMA block. With increasing PDMA block size the hydrodynamic diameter increases noticeably while the hydrophobic polystyrene block

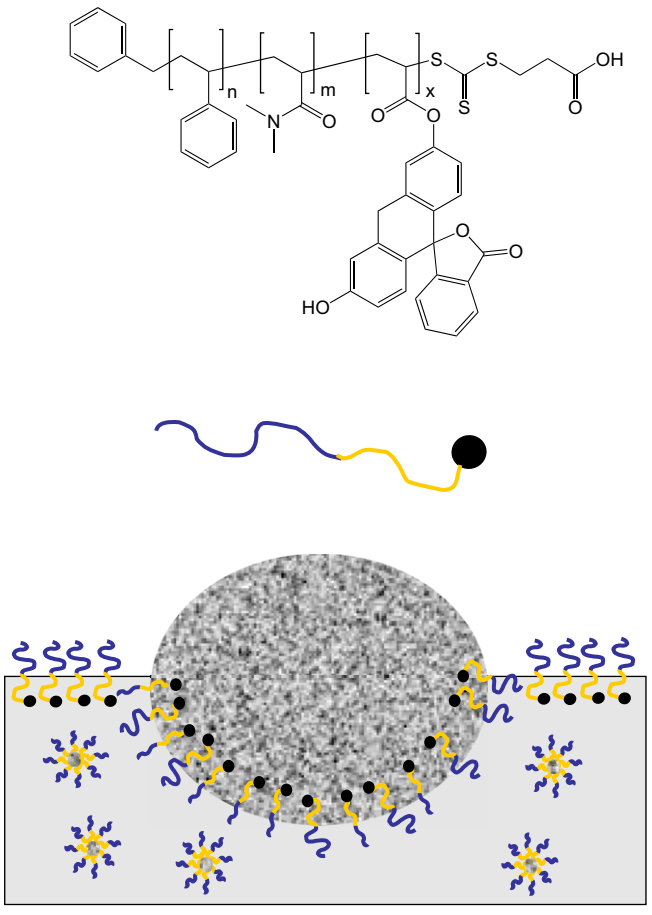

Scheme 3.

has only a minor influence. The size of the inverse micelle increased only gradually with the size of the hydrophobic shell-forming block (Fig. 8). According to the model developed by Halperin [42] we can fit the dependency between the number of repeating units N of both blocks, N_{PS} and N_{PDMA}, and the hydrodynamic diameter D_h to approximately $D_h \propto N_{PS}^{0\pm0.1} \cdot N_{PDMA}^{1\pm0.05}$. However, the very small hydrodynamic diameter – especially when looking at PDMA blocks below 100 repeating units (Fig. 8) – suggest that the aggregation number is either extremely small or only unimers are present. In fact, the critical micelle concentration (cmc) in organic solvent is rather high and only a significantly high PDMA block ratio can lead to a small cmc [43,44].

Water was subsequently added and the solution mixture was shaken for 2 s and analyzed immediately. The hydrodynamic diameter D_h was measured every 10 s using dynamic light scattering (DLS) analysis. Several replicated experiments were conducted to eliminate uncertainties derived from short measurement times. The measured hydrodynamic diameter was observed to increase immediately resulting in micelle diameters of more than 50 nm (Fig. 9). The micelles are now swollen with water, with a considerable increase in aggregation number can also be expected [45]. Closer inspection allows the correlation between block sizes and diameter increase. Within acceptable errors, the rate of swelling was solely dependent on the hydrophilic PDMA block (Fig. 9). The typical casting process lies within similar time frames of up to 1 min. It can therefore be expected that the longer the PDMA block – independent of the size of the hydrophobic block – the more water was encapsulated inside the core of micelle.

From these results, it became evident that a long hydrophilic block may significantly interfere with the casting condition. By lowering the interfacial tension a stronger tendency of droplet coalescence can be expected. Furthermore, water may be taken up by the micelle leading to a competing process next

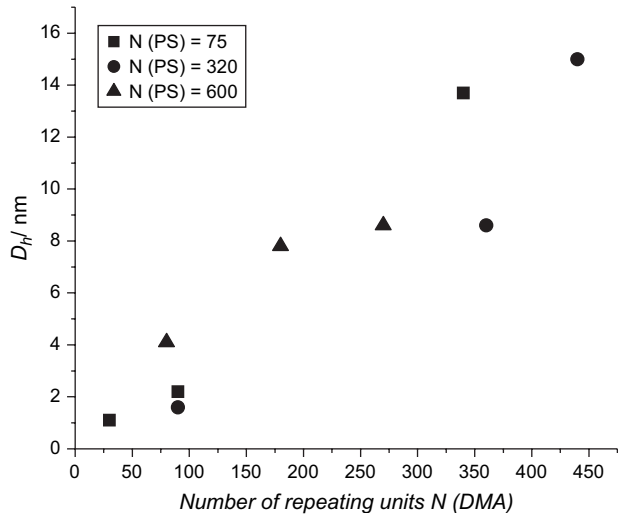

Fig. 8. Hydrodynamic diameter (D_h) as obtained *via* DLS in methylene chloride (10 g L^{-1}) in correlation with the theoretical number of repeating units N of the PDMA block.

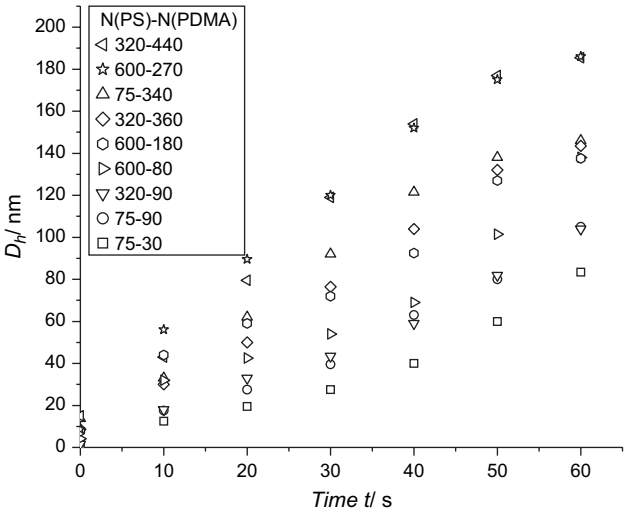

Fig. 9. Increase of hydrodynamic diameter D_h *vs* time as a result of water uptake caused by shaking a solution of PS-*b*-PDMA (10 g L^{-1} in methylene chloride) with water.

to the honeycomb formation. It should also be mentioned that a hydrophilic block delays the precipitation of polymer around the water droplets while capturing their shape, which is an essential step in the formation process of honeycomb structured porous films. An optimum balance between hydrophilic and hydrophobic block is expected to be a prerequisite. In addition, the casting conditions, especially the humidity, is expected to be very influential to the regularity of pores formed.

4.4. Casting under varying humidity

As established, the pores generated in porous films were due to a natural templating of water droplets, condensed onto the surface of the polymer solution during evaporation of solvent. These water droplets came from the surrounding humid environment, which were introduced during casting. Hence, the humidity in the environment determines the availability of moisture to form water droplets.

During our investigations, castings were completed in a customized Perspex glove box, setup at humidity levels ranging between 50 and 90%, and all other parameters were kept constant. As depicted in Fig. 10, films generated using PS_{75}-*b*-$PDMA_{30}$, at humidity of 50%, have no visible pores. As the humidity increases to 60%, tiny and non-homogeneous pores of sizes between 250 and 750 nm were formed with a faint suggestion of honeycomb arrangements of pores. At humidity levels of 65%, highly homogeneous pores of 1 μm arranged in honeycomb fashion were formed while further increase in humidity to 80% only yielded an increase in pore sizes with ruined honeycomb arrangements of pores. When the humidity was further increased to 90%, the pores formed were vastly large, non-homogeneous, and very different in sizes with the honeycomb porous arrangement totally blemished. This vogue was evident in all block ratios of PS-*b*-PDMA copolymers investigated in this study. Since qualitative analysis of these films is rather subjective a quantitative analysis technique –

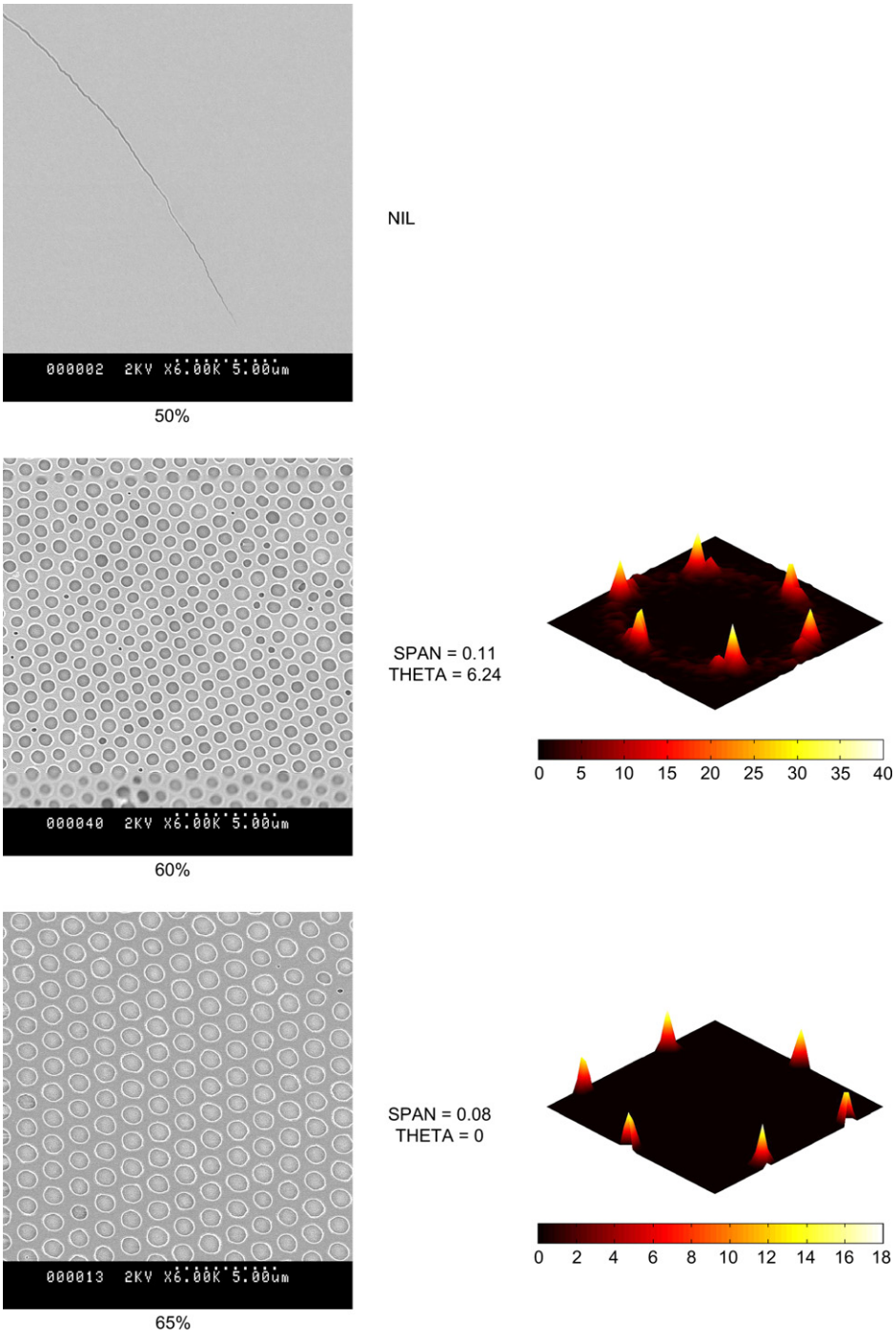

Fig. 10. SEM images of porous films from block copolymer PS_{75}-*b*-$PDMA_{30}$ obtained from a polymer solution (10 g L^{-1}) of 70:30 v/v%, CS_2/CH_2Cl_2 at constant airflow and varying humidity (50–90%).

quantified virtual light scattering, which is based on Fourier transformation – has been employed [7,33,34]. The result of this analysis is depicted in Fig. 10 confirming the increased disorder.

These observations can be consequences of the quantity of moisture in the environment available for water droplet formation. At low humidity, the availability of moisture concentration was not sufficient to form droplets on the solution surface. At higher humidity, these water droplets can increase in size before polymer precipitation into solid layers around the droplet. However, when the humidity was excessive, the downward airflow draft of moisture leading to condensing water droplets on the surface may be surplus. As a result, high volume of moisture results in an increasing size of water droplets. This can happen so rapidly and cause water droplets to coalesce before precipitation of the polymer around the droplets occur. This behavior is in strong contrast to hydrophobic polymers. An increasing humidity always seemed to improve

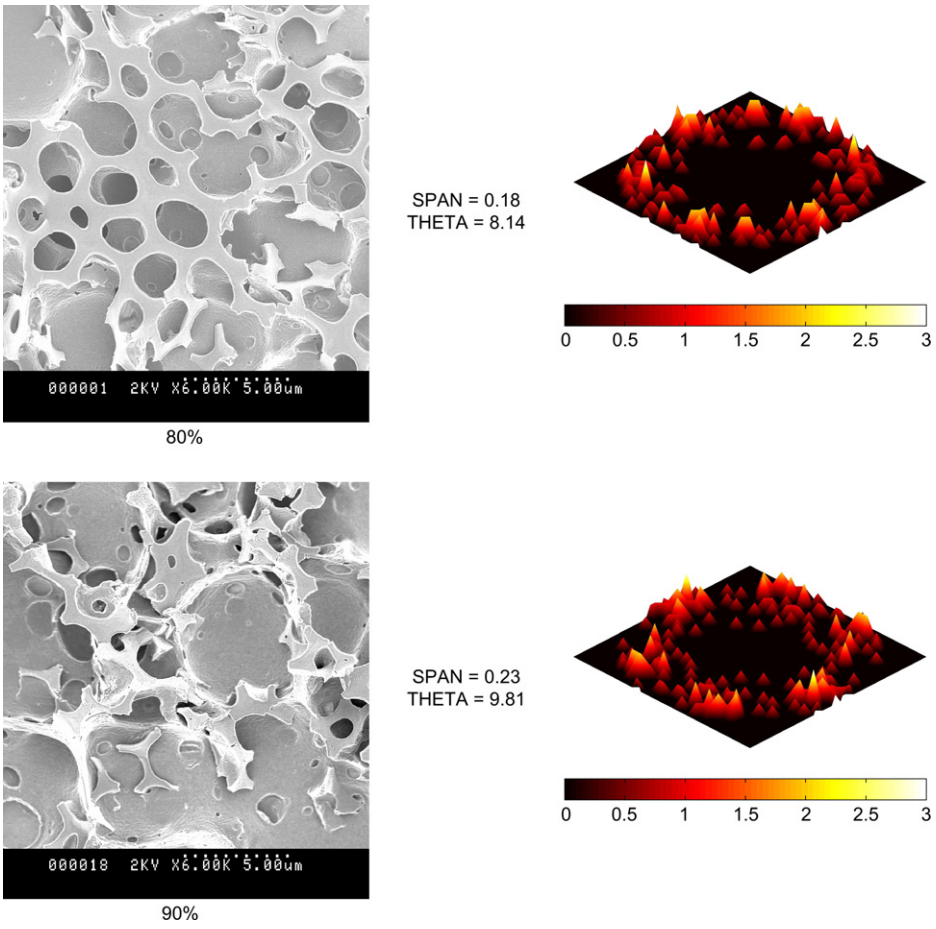

Fig. 10 *(continued)*.

the regularity. Amphiphilic block copolymers, however, are hygroscopic and do interact with water during the casting process as discussed. The difficulty with increasingly hydrophilic polymers became evident in the investigation of polymers with increasing ratio of DMA in the block copolymer. As depicted in Fig. 11, porous films generated from PS_{75}-*b*-$PDMA_{30}$, PS_{75}-*b*-$PDMA_{90}$, PS_{75}-*b*-$PDMA_{340}$, an increasing hydrophilic PDMA block size or ratio to PS block, resulted in lower regularity. This is easily assigned to the enhanced uptake of water droplets with larger hydrophilic PDMA blocks. However,

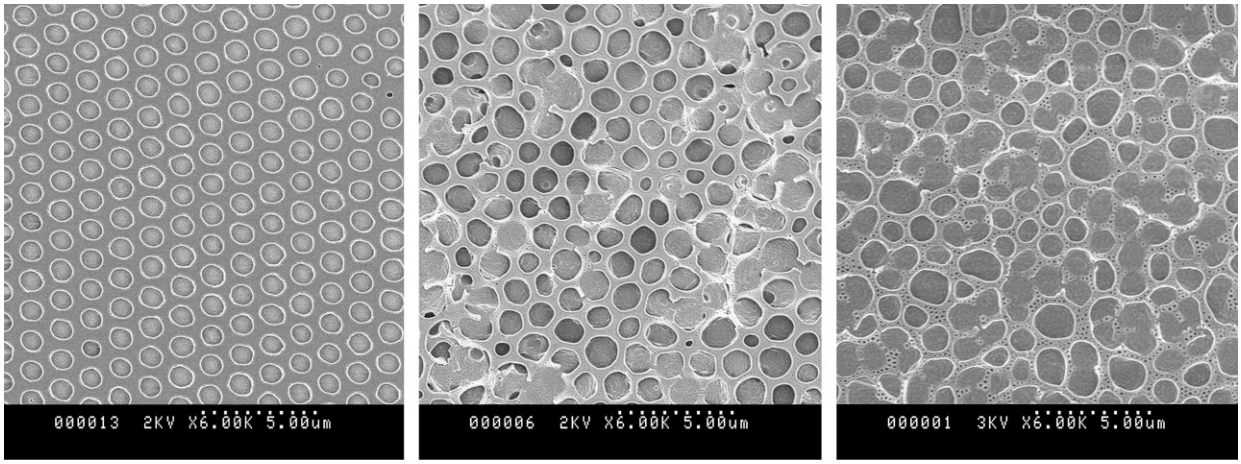

Fig. 11. SEM images of porous films from block copolymer PS-*b*-PDMA obtained from a polymer solution (10 g L^{-1}) of 70:30 v/v%, CS_2/CH_2Cl_2. The images depict the best possible pores regularity in correlation with the size of the PDMA block.

when the PDMA blocks were excessively huge, the uptake can be so explosive with water droplets increasing in size so rapidly and coalesce with each other before surrounding polymers can precipitate into solid, tarnishing the honeycomb arrangements and homogeneity of pores created initially. This vogue was also observed in other block ratios of PS-*b*-PDMA copolymers in this study.

Another remarkable observation in this humidity study was the influence of block ratios and size of PDMA blocks in PS-*b*-PDMA copolymers employed. As depicted in Fig. 11, porous films generated from PS_{75}-*b*-$PDMA_{30}$, PS_{75}-*b*-$PDMA_{90}$, PS_{75}-*b*-$PDMA_{340}$, with an increasing hydrophilic PDMA block size or ratio to PS blocks the humidity required to generate the best possible honeycomb structured porous films was found to be lower (PS_{75}-*b*-$PDMA_{30}$ = 65%, PS_{75}-*b*-$PDMA_{90}$ = 60%, PS_{75}-*b*-$PDMA_{340}$ = 50%). This is easily assigned to the enhanced uptake of water droplets with larger hydrophilic PDMA blocks.

4.5. Casting under varying airflow rate

The time permitted for condensation of water droplets onto the casting polymer solution is subjected to the evaporation rate of solvent from the casting polymer solution.

A high airflow rate of moist air supplied increases the evaporation rate of solvent, plummeting the opportunities for appropriate condensation. Very small pore sizes were in fact observed at very high air flows especially when combined with a low solvent volume [5]. At the same time, a high airflow rate of moist air supplied also resulted in additional moisture and can result in opposite effects.

A correlation study of the airflow rate of moist air to the morphology of porous films generated was obtained with castings completed in a dry glove box setup (humidity $< 25\%$) with moist air supplied from a funnel and directed over the casting at a fixed humidity (85%), controlled at various airflow rates. The low humidity in the glove box is essential to prevent initial inceptions of unwanted condensations taking place before moist air is introduced.

Fig. 12 presents porous films generated using PS_{75}-*b*-$PDMA_{90}$ at various airflow rates of moist air. At zero airflow rates, 0 L min^{-1}, no pores or non-homogeneous insignificant pores were generated on the film. This can be assigned to a superior upwards draft of evaporating solvent vapors that may have prevented the downward draft of moist air settling onto the casting polymer solution for condensation into water droplets to happen. When the airflow rate was raised to 0.2 L min^{-1}, highly ordered pores with homogeneous pore size of 1.5 μm are generated. When the airflow rate was increased further from 0.4 to 0.8 L min^{-1}, the size of pores generated also increased to 1.7 and 3.1 μm. The increase in airflow rate of supplied moist air seemed to have aided the condensations and swelling of water droplets on the casting polymer solution even with an increased evaporation rate of solvent. Unfortunately, at 1 L min^{-1} airflow rate of supplied moist air, the elegant honeycomb arrangement and homogeneous pore sizes generated previously are devastated. This can be assigned to a surplus of moisture contributing into swelling the water droplets so rapidly that coalescing of water droplets took place before the copolymer precipitated, ruining the size homogeneity and hexagonal arrangement of pores.

Another observation established in this study of airflow rate of moist air, is the effect of the ratio of PDMA blocks to the PS blocks in copolymers employed. It was observed that with a higher ratio of PDMA block to PS block the formation of pores and honeycomb arrangement can only be achieved with a low airflow rate of supplied moist air. As depicted in Fig. 13, porous films generated from PS_{75}-*b*-$PDMA_{30}$, PS_{75}-*b*-$PDMA_{90}$ and PS_{75}-*b*-$PDMA_{340}$, respectively, the airflow rate of moist air supplied to generate honeycomb structured porous films with comparable pore sizes is lower. It is possible to attribute this to a promoted and enhanced uptake of water droplets by the larger block of PDMA, even at higher evaporation rate of solvent.

4.6. Effect of block sizes

The results as presented in Figs. 10–13 indicated a strong influence of the block sizes on the castings outcome. While the size of the hydrophobic PS block played only a negligible role, with pores typically decreasing slightly in size with decreasing block size used, the hydrophilic block interferes significantly with this water driven process. In general, a lengthy hydrophilic block impedes the formation of highly regular films and the resulting porous array is usually of lower order. However, reducing the moisture content of the environment either by lowering the humidity in the casting environment or by reducing the rate of the airflow allows significant improvement of the regularity. These results can be seen in connection with the interaction of water and PDMA block. The lower surface tensions as well as the higher tendency to take up water are aspects preventing the formation of hexagonal arrays. While it is possible to obtain regular films with any block ratio, a high PDMA content requires careful fine-tuning of the casting parameters concerning the humidity.

4.7. Internal structure of the pores

The resulting honeycomb structured films do have a closed pore structure. It has been demonstrated earlier that typical preparation techniques result in multi-layers of closed pores [6]. A more membrane-like open pore structure is usually obtained by the presence of surface active compounds such as polyelectrolytes [46,47].

The interaction of the amphiphilic polymer with water droplets superimposes a nano-structure onto the apparent honeycomb microstructure. As mentioned earlier, the block copolymer can possibly rearrange around the micron-sized pore-forming water droplet. As a consequence, the resulting pore should possess a hydrophilic surface. Secondly, water can penetrate into the micelles formed by the polymer, leading to water swollen particles.

The uptake of water into the micelle can indeed be confirmed upon closer investigation of the final honeycomb

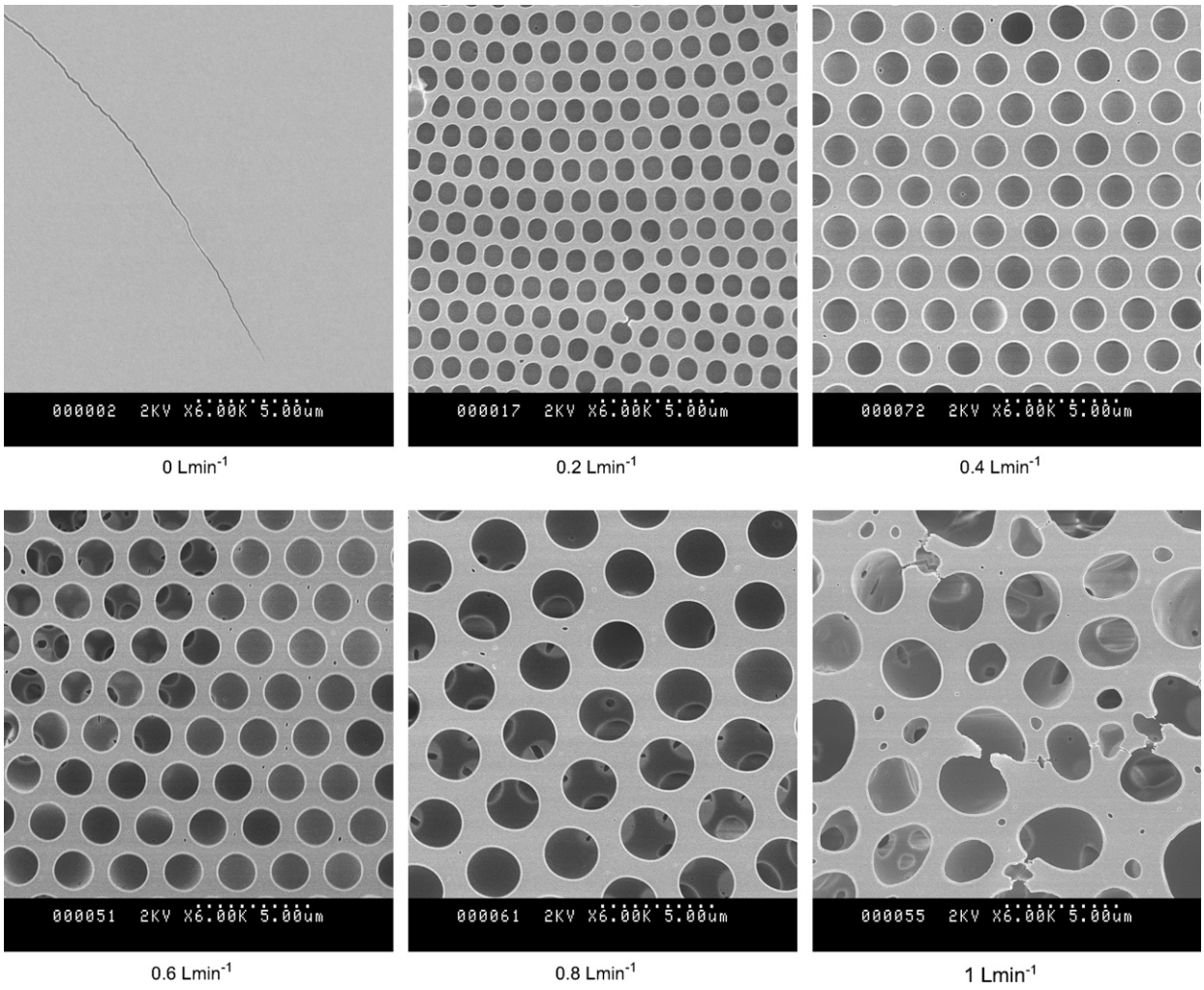

Fig. 12. SEM images of porous films from block copolymer PS_{75}-*b*-$PDMA_{90}$ obtained from a polymer solution (10 g L^{-1}) of 70:30 v/v%, CS_2/CH_2Cl_2 at varying air flows and a constant humidity of 85%.

structured porous films. With increasing hydrophilic block length the appearance of nano-sized pores became more evident. These nanopores can be found throughout the films such as on the film surface or within the micron-sized pores (Fig. 14). The size of these nanopores can be correlated to the size of the water swollen micelles (Fig. 9). It seems that

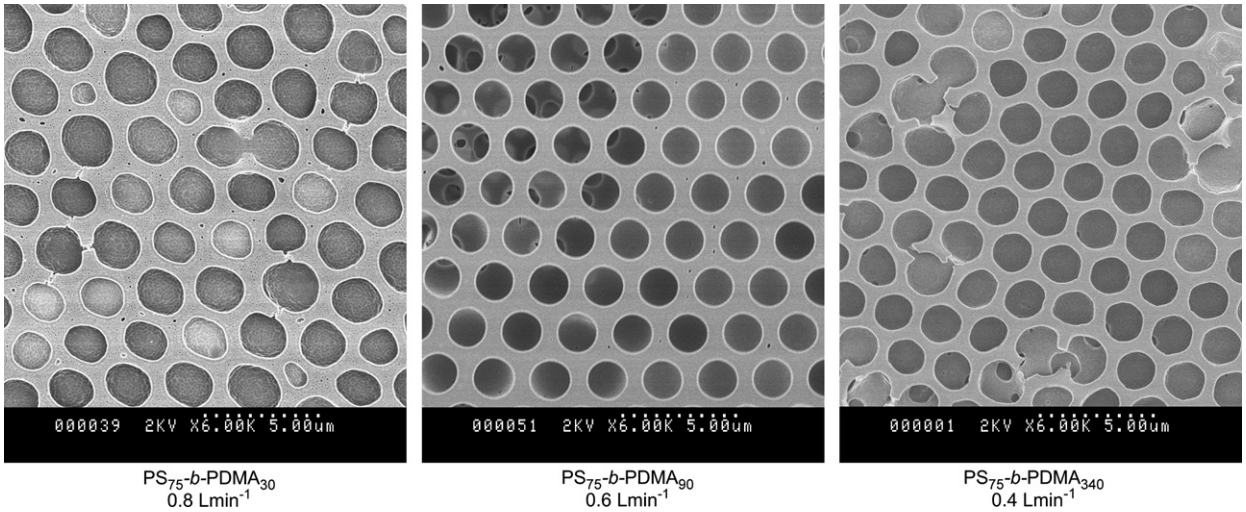

Fig. 13. SEM images of porous films from block copolymers with varying PDMA block lengths obtained using optimized airflow rate. Polymer solution (10 g L^{-1}) of 70:30 v/v%, CS_2/CH_2Cl_2 and at constant humidity of 60%.

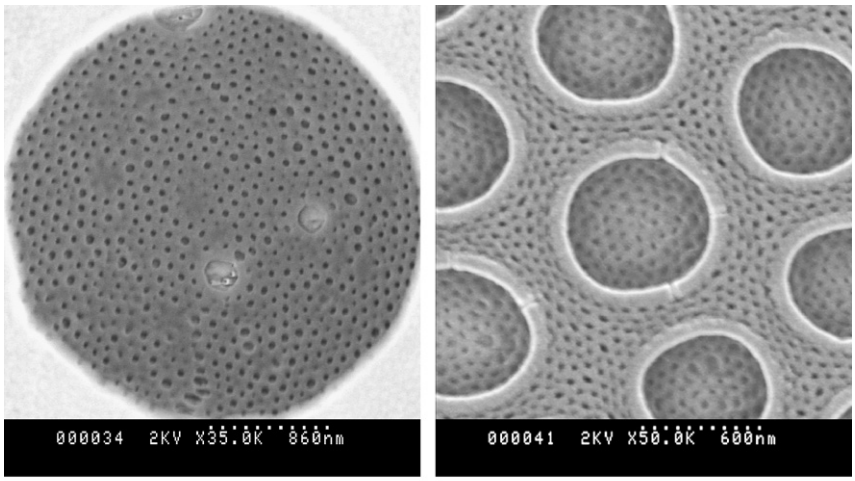

Fig. 14. SEM images of a typical internal structure of porous films prepared from block copolymers with large hydrophilic blocks, showing both micro-pores and nanopores.

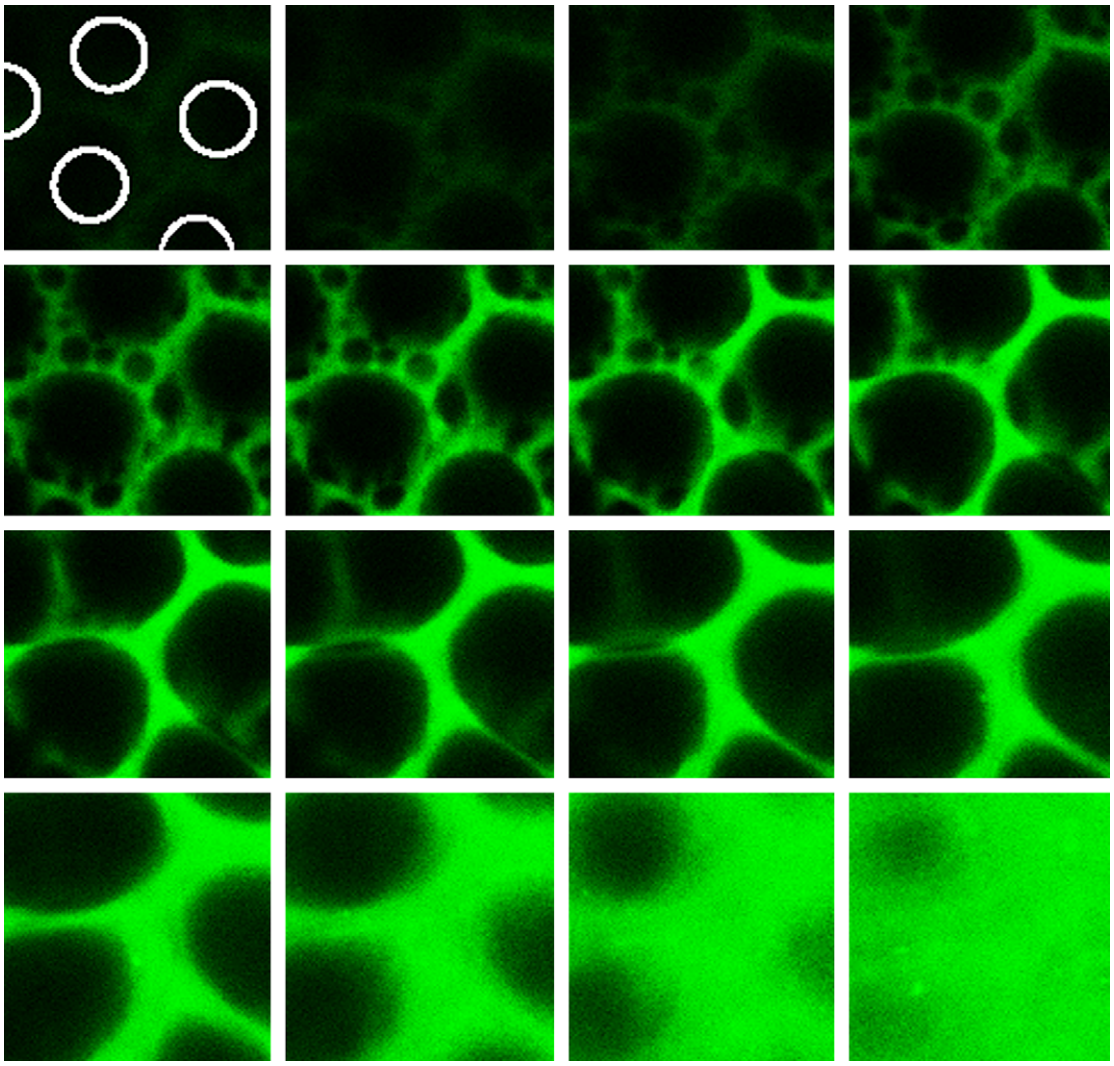

Fig. 15. Confocal microscope of a PS-*b*-PDMA block copolymer porous film with fluorescence labeled hydrophilic block. The sections in the *z*-axis are 100 nm starting from the surface of the film (with the highlighted position of the pore) (upper left) until a penetration into the film of 1.6 μm (lower right).

two competing processes are taking place during the casting process. Micro-sized droplets lead to the formation of pores while excess water is encapsulated within the pores. As a result, a highly porous surface with pores on micron- and nano-size is obtained.

A further nano-scaled suborder is derived from the rearrangement of amphiphilic block copolymers around the micron-scaled water droplet. This arrangement is expected to be captured in its current state after the evaporation of solvent and water. Consequently, these nano- and micron-pores should have a hydrophilic surface while the overall surface of the film usually remains hydrophobic, hence, being enriched with styrene. To test this hypothesis, XPS [19] and bacterial adhesion [3] studies were employed to validate this hypothesis. Further confirmation can be obtained by using confocal microscopy studies to obtain more information on the internal structure. A block copolymer PS-*b*-PDMA prepared with RAFT agent **II** was further chain extended with a few units of fluorescein *o*-acrylate (Scheme 3). The resulting fluorescing tri-block copolymer was employed during the casting process to mark the location of the hydrophilic block. Investigations using the confocal fluorescence microscope showed the absence of significant fluorescence on the surface of the film (Fig. 15). The surface is therefore enriched with the hydrophobic polystyrene block. The white rings in Fig. 15 indicated the location of the pores on the surface. Penetration analysis into the polymer film showed an immediate increase in the fluorescence intensity and rises even more with increasing depth into the sample along the *z*-axis. The pores are now clearly visible as dark spots. Between the micron-sized pores, nano-sized dark areas appear. The origin of these dark spots can either be as mentioned previously pores (caused by swelling of micelles with water) or can be an indication of nano-phase separation of two immiscible polymer blocks. Further penetration along the *z*-axis leads to the bottom of the pore showing an intense fluorescence stain. While these results alone do not confirm the presence of hydrophilic pores, in combination with earlier experiments [3] superimposed nano-scaled suborder can indeed be anticipated.

5. Conclusion

In conclusion, the formation of porous films with the desired pore size and pore arrangement using the breath figure technique is a multifaceted procedure. With numerous parameters, both physical and chemical affecting the formation, delicate selection of each parameter and their combinations are mandatory to provide the best environment and conditions to generate the required film with desired structural properties. Any excessive conditions will ruin either the size homogeneity of pores or the hexagonal arrangement of pores formed. In addition, manipulations to the physical aspect of casting can only offer partial adjustments to the pore size formed without upsetting the hexagonal arrangement of pores. On the contrary, the chemical aspect is the primary element that can provide major changes to the size of pores while preserving the hexagonal arrangement. As such, to have honeycomb with large or small pores, alteration to the chemical aspect, such as a different selections of polymer with different architectures, molecular weight, chain length, solvent used or polymer concentrations, can give the desired pore size. The observation of another population of nanopores on the surface and within the pores of honeycomb, structured porous films generated provided certain insight into the probable arrangements of PS-*b*-PDMA, on the surface and inside the macro-pores within the solid film generated.

Acknowledgements

We would like to thank the Australian Research Council (ARC) for a Discovery grant and a scholarship for K.H. Wong, Mr. Gavin McKenzie of the Histology and Microscopy Unit of the School of Medical Sciences for his help with the confocal microscopy analyses. Maribel Hernández-Guerrero for discussions and Mr. Istvan Jacenjik for his excellent management of the research centre (CAMD).

References

[1] Widawski G, Rawieso M, François B. Nature 1994;369:387–9.
[2] Stenzel MH. Aust J Chem 2002;55:239–43.
[3] Stenzel MH, Barner-Kowollik C, Davis TP. J Polym Sci Part A Polym Chem 2006;44:2363–75.
[4] Bunz UHF. Adv Mater 2006;18:973–89.
[5] Yabu H, Shimomura M. Chem Mater 2005;17:5231.
[6] Srinivasarao M, Collings D, Philips A, Patel S. Science 2001;292:79–83.
[7] Hernández-Guerrero M, Barner-Kowollik C, Davis TP, Stenzel MH. Eur Polym J 2005;41:2264–77.
[8] Jenekhe SA, Chen X. Science 1998;279:1903–7.
[9] Song L, Bly RK, Wilson JN, Bakbak S, Park JO, Srinivasarao M, et al. Adv Mater 2004;16:115–8.
[10] Erdogan B, Song LL, Wilson JN, Park JO, Srinivasarao M, Bunz UHF. J Am Chem Soc 2004;126:3678–9.
[11] Wong KH, Davis TP, Barner-Kowollik C, Stenzel MH. Aust J Chem 2006;59:539–43.
[12] Yabu H, Tanaka M, IJiro K, Shimomura M. Langmuir 2003;19:6297–300.
[13] Barner-Kowollik C, Dalton H, Davis TP, Stenzel MH. Angew Chem Int Ed 2003;42:3664–8.
[14] Hao X, Stenzel MH, Barner-Kowollik C, Davis TP, Evans E. Polymer 2004;45:7401–15.
[15] Englert BC, Scholz S, Leech PJ, Srinivasarao M, Bunz UHF. Chem Eur J 2005;11:995–1000.
[16] Nishikawa T, Nonomura M, Arai K, Hayashi J, Sawadaishi T, Nishiura Y, et al. Langmuir 2003;19:6193–201.
[17] Karthaus O, Maruyama N, Cieren X, Shimomura M, Hasegawa H, Hashimoto T. Langmuir 2000;16:6071–6.
[18] Karikari AS, Williams SR, Heisey CL, Rawlett AM, Long TE. Langmuir 2006;22:9687–93.
[19] Stenzel MH, Davis TP. Aust J Chem 2003;56:1035–8.
[20] Nygard A, Barner-Kowollik C, Davis TP, Stenzel MH. Aust J Chem 2005;58:595–9.
[21] Perrier S, Takolpuckdee P. J Polym Sci Part A Polym Chem 2005;43:5347–93.
[22] Barner-Kowollik C, Davis TP, Heuts JPA, Stenzel MH, Vana P, Whittaker M. J Polym Sci Part A Polym Chem 2003;41:365–75.
[23] Moad G, Rizzardo E, Thang SH. Aust J Chem 2005;58:379–410.
[24] Yusa S, Shimada Y, Mitsukami Y, Yamamoto T, Morishima Y. Macromolecules 2003;36:4208–15.

[25] Arotcarena M, Heise B, Ishaya S, Laschewsky A. J Am Chem Soc 2002;124:3787–93.
[26] Stenzel MH, Barner-Kowollik C, Davis TP, Dalton HM. Macromol Biosci 2004;4:445–53.
[27] Save M, Manguian M, Chassenieux C, Charleux B. Macromolecules 2005;38:280–9.
[28] Garnier S, Laschewsky A. Macromolecules 2005;38:7580–92.
[29] Mertoglu M, Garnier S, Laschewsky A, Skrabania K, Storsberg J. Polymer 2005;46:7726–40.
[30] Convertine AJ, Lokitz BS, Vasileva Y, Myrick LJ, Scales CW, Lowe AB, et al. Macromolecules 2006;39:1724–30.
[31] Wong KH, Hernández-Guerrero M, Granville AM, Davis TP, Barner-Kowollik C, Stenzel MH. J Porous Mater 2006;13:213–23.
[32] Le TP, Moad G, Rizzardo E, Thang SH. International Patent PCT WO 9801478; 1998.
[33] Angus SD, Davis TP. Langmuir 2002;18:9547.
[34] Lord HT, Quinn JF, Angus SD, Whittaker MR, Stenzel MH, Davis TP. J Mater Chem 2003;13:2819.
[35] Feldermann A, Coote ML, Stenzel MH, Davis TP, Barner-Kowollik C. J Am Chem Soc 2004;126:15915–23.
[36] Xu J, He J, Fan D, Tang W, Yang Y. Macromolecules 2006;39:3753–9.
[37] Quinn JF, Barner L, Barner-Kowollik C, Rizzardo E, Davis TP. Macromolecules 2002;35:7620–7.
[38] Albertin L, Stenzel MH, Barner-Kowollik C, Davis TP. Polymer 2006;47:1011–9.
[39] Vana P, Albertin L, Davis TP, Barner L, Barner-Kowollik C. J Polym Sci Polym Chem 2002;40:4032–7.
[40] Pai TSC, Barner-Kowollik C, Davis TP, Stenzel MH. Polymer 2004;45:4383–5392.
[41] Monteiro MJ. J Polym Sci Part A Polym Chem 2005;43:5643–51.
[42] Halperin A. Macromolecules 1987;20:2943–6.
[43] Chu B, Zhou Z, Wu G. J Non-Cryst Solids 1994;172–174:1094–102.
[44] Hilfiker R, Chu B, Xu J. J Colloid Int Sci 1989;133:176–84.
[45] Vagberg LJM, Cogan KA, Gast AP. Macromolecules 1991;24:1670–7.
[46] Yabu H, Hirai Y, Shimomura M. Langmuir 2006;22:9760–4.
[47] Yabu H, Shimomura M. Langmuir 2006;22:4992–7.